

This item is the archived peer-reviewed author-version of:

LoRay : AoA estimation system for long range communication network

Reference:

Bni Lam Noori, Joosens Dennis, Aernouts Michiel, Steckel Jan, Weyn Maarten.- LoRay : AoA estimation system for long range communication network
IEEE transactions on wireless communications / Institute of Electrical and Electronics Engineers [New York, N.Y.] - ISSN 1536-1276 - 20:3(2021), p. 2005-2018
Full text (Publisher's DOI): <https://doi.org/10.1109/TWC.2020.3038565>
To cite this reference: <https://hdl.handle.net/10067/1739530151162165141>

LoRay: AoA Estimation System for Long Range Communication Networks

Noori BniLam^{1,4}, Dennis Joosens¹, Michiel Aernouts¹, Jan Steckel^{2,3}, Maarten Weyn¹

¹University of Antwerp - imec, IDLab - Faculty of Applied Engineering, Sint-Pietersvliet 7, 2000 Antwerp, Belgium

²University of Antwerp, Cosys-lab Research Group, Antwerp, Belgium

³Flanders Make Strategic Research Center

⁴ Corresponding author: noori.bniam@uantwerpen.be

Abstract—In this paper, we introduce a comprehensive angle of arrival (AoA) estimation solution for the long range (LoRa) communication network. Termed the LoRa array (LoRay), the proposed system constitutes hardware and software solutions to estimate the AoA of the received signals in real life urban environments. The hardware solution is based on converting multiple individual software defined radios (SDR) into a single SDR that consists of multiple RF-channels. The proposed hardware is cost effective, flexible and generic. The software solution, on the other hand, utilizes the space alternating generalized expectation-maximization (SAGE) algorithm to estimate the AoA of highly correlated received signals. The proposed software exploits few samples of the received signal to estimate the AoA of the direct and reflected paths in an intensive multipath environment. The LoRay system has been validated in outdoor urban environments. The experimental results show that the proposed system provides stable and accurate AoA estimations for both the line-of-sight (LoS) and the non-line-of-sight (NLoS) conditions. The AoA of 80% of the received signals have been estimated within an estimation error below 2° and 10° for the LoS and the NLoS locations, respectively.

Index Terms— angle of arrival, AoA, direction of arrival, DoA, direction finding, DF, LoRa, LoRaWAN, LPWAN, outdoor AoA estimation, IoT localization.

I. INTRODUCTION

Over a decade ago, the low power wide area networks (LPWAN) have emerged to provide the communication requirements that enabled the Internet of Things (IoT) concept. Therefore, recently, futuristic ideas that are based on the IoT concept (e.g. smart cities, smart highways, smart farms, etc...) have become a reality. This communication revolution can be attributed to the LPWAN capability of establishing long range communication links (up to several kilometers) using low power consumption transceivers. This is possible due to the fact that IoT messages are usually very short (e.g. temperature data, CO2 level, motion information, etc), thus, a narrowband transmission is sufficient for this purpose. Moreover, due to the low production cost of narrowband transceivers, the LPWAN transceivers are expected to be massively deployed on large scale environments; i.e. cities and countries.

Consequently, locating the massive amount of transceivers is considered a key feature that distinguishes LPWAN technologies from each other. For instance, the Sigfox and NB-IoT networks can provide localization solutions based on the

received signal strength (RSS) values [1], [2]. The LoRa network, on the other hand, can provide a localization solution based on the time difference of arrival (TDoA) of the received signals [3]. Recently, few promising attempts were introduced that combine the TDoA estimations with the angle of arrival (AoA) estimations to provide a localization solution for LoRa networks [4], [5].

The exploitation of the LPWAN signals' characteristics (i.e. the narrow bandwidth and the minimal transmission power) by a localization solution can be a very challenging task. For instance, the RSS-based localization accuracy, due to the low transmitted power and the expected long communication links, might decline rapidly on account of the multipath propagation and the wireless communication channel fading. Time-based localization solution, on the other hand, provides a limited localization accuracy due to the limited bandwidth of the transmitted signals. The AoA-based localization solution, however, seems to be the only possible technique that can utilize the LPWAN signals' characteristics without enduring a fundamental penalty. The AoA estimation technique estimates the angle between the transmitter and the receiver by measuring the phase of the received signal at different points in space; using array antennas. Consequently, the narrow operating bandwidth of the LPWAN signals will provide a unique phase response, hence, achieving an accurate AoA estimation. Moreover, the AoA estimation approach does not depend directly on the received signal strength, thus, the effect of the wireless communication channel fading, relative to the RSS-based localization solution, is minimal. Furthermore, unlike the RSS and time-based localization solutions, the AoA estimation technique can decompose the received signals into direct and reflected paths, thus, the multipath effect can be minimized. Despite all these merits, commercially available AoA-based localization systems for LPWAN technologies (to the best of the authors' knowledge) do not yet exist. This absence can be attributed to the high deployment's cost and complexity that is associated with the AoA estimation systems. Therefore, promoting AoA-based localization solutions for the LPWAN technologies can only be achieved by reducing the production cost and simplifying the system complexity, which constitutes the main objective of this paper.

AoA-based localization approach requires multiple spatially distributed AoA estimation systems in the vicinity of the

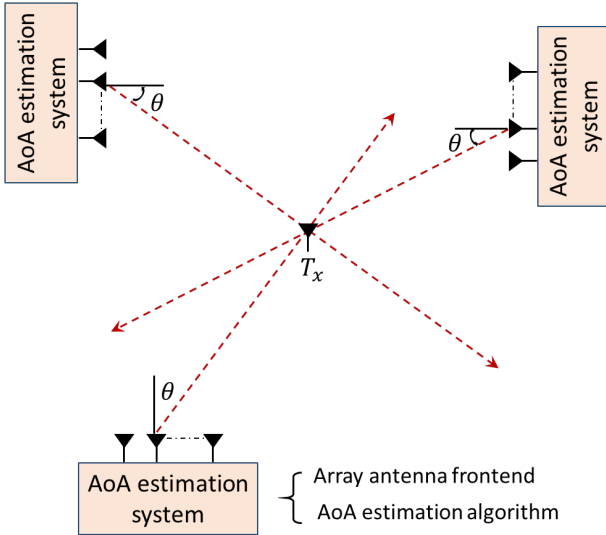


Fig. 1: A schematic representation of the AoA-based localization solution. The figure shows that the AoA-based localization solution requires multiple spatially distributed AoA estimation systems. Every AoA estimation system can provide the direction of the transmitting device. Combining the direction information can provide a location estimate of the transmitting device.

transmitting device, as shown in Fig. 1. Every AoA estimation system, which constitutes an array antenna frontend and an AoA estimation algorithm, can estimate the direction of the transmitting device. Combining the direction information from every AoA estimation system can provide a location estimate of the transmitting device [6]. In this paper, we introduce an AoA estimation system that is suitable for LPWAN technologies in general and LoRa communication network in specific. The proposed system is cost effective (it is built based on low cost components), flexible (It does not impose any restrictions or assumptions), generic (it is independent of the array antenna structure) and it requires minimal computational power to provide the AoA estimates of the received signals. Therefore, the proposed system is a serious attempt that might lead to mass deployments of AoA-based localization solutions with LPWAN technologies.

In the following subsections, we will provide an overview of the existing array antenna frontends for LPWAN technologies, a brief overview of the available AoA estimation algorithms, and finally the contributions and the layout of this paper.

A. Array Antenna Frontends

As stated earlier, any AoA estimation system requires the deployment of an array antenna frontend at the receiver side. Lately, several array antennas, that can provide AoA estimations for LPWAN technologies, have been proposed. Steckel et al. [7] provided a hardware architecture which imposes random projection weights that are required for the compressive sensing optimization. Their hardware architecture increases the array antenna aperture (i.e. it increases the array degrees of freedom) without increasing the amount of the RF-channels. The solution has certainly merits, nevertheless, they tested the hardware only in an anechoic chamber, therefore, the

solution performance needs to be evaluated in a real life environment. The solution also requires a random distribution of the antenna elements in space, thus, it might lead to an increase of the array antenna physical size, hence, the deployment flexibility of this solution is not guaranteed. Furthermore, they utilized a high cost off-the-shelf software defined radio (SDR) frontend [8] (which constitutes two coherent RF-channels) to extract the phase information. Consequently, the high cost and the lack of flexibility make this solution less suitable for mainstream or large-scale applications.

BniLam et al. [9] provided a software solution that combines several small array antennas into a single large array antenna. They validated the solution performance in a real life outdoor environment with DASH7¹ communication standard [10]. The experimental results revealed that the proposed augmented array antenna provides more accurate AoA estimates than the individual small array antennas. Nevertheless, they utilized the same off-the-shelf SDR that has been adopted in [7]; rendering the solution as a high cost setup.

Baik et al [11] have provided an AoA estimation solution based on a time modulated array (TMA) that consists of two antenna elements. They validated their solution with LoRa signals in an outdoor football field, where only the line-of-sight (LoS) condition was considered. Even though, their solution has enabled a single RF-channel SDR to estimate the AoA of a received signal, the small array antenna aperture (only two antenna elements) can only provide an AoA estimate of a single received path. Therefore, the estimation accuracy might severely deteriorate in an urban environment where the multipath effect is inevitable.

Avitabile et al. [12] have provided a low cost and complexity hardware solution to estimate the AoA of a single received signal. They manufactured an array antenna, which constitutes four antenna elements, and they validated it experimentally. The experimental results were very accurate when the transmitter was placed within less than 5 meters away from the hardware solution. The hardware works under the assumption of a single received signal; thus (similar to [11]) its performance may severely deteriorate in a realistic environment that is full with multipath components.

Recently, we introduced the RTL-Array prototype as a low cost hardware that can provide AoA estimations of the received signals [13]. The prototype was built based on converting 6 individual low cost SDR frontends (called the RTL-SDR [14]) into a single SDR that consists of 6 RF-channels. These RF-channels are synchronized in time and frequency, and coherent in phase. The prototype has been tested in an anechoic chamber with DASH7 received signals. The experimental results show that the RTL-Array provides a very stable and accurate phase response for the received signals. Nevertheless, the prototype has not been validated in a real life environment. Moreover, the prototype has not been tested with an AoA estimation algorithm. In this paper, however, we tackle these two issues to provide a flexible and low cost AoA estimation

¹DASH7 is an open source mid-range communication standard for IoT applications. Its physical layer utilizes the Gaussian Frequency Shift Keying GFSK modulation scheme and it operates in the unlicensed sub-1 GHz bands.

system for LPWAN technologies that can estimate the AoA of the direct and reflected paths of the received signal in an urban environment.

B. AoA Estimation Algorithms

Over the years, several AoA estimation algorithms have been proposed [15]. In general, these algorithms can be classified into four main categories:

- i) Algorithms that are based on the array antenna beamforming (BF) technique; e.g. minimum variance distortionless response (MVDR) beamformer [16].
- ii) Algorithms that rely on the signal and noise subspace decomposition (SD) technique; e.g. multiple signal classification (MUSIC) [17], Root-MUSIC [18], estimation of signal parameter via rotational invariance technique (ESPRIT) [19] and unitary ESPRIT [20].
- iii) Algorithms that apply the sparse representation of space (SRS); e.g. focal underdetermined system solver (FOCUSS) [21], sparse-based optimization [22] and compressive beamforming [23].
- iv) Algorithms that employ a parametric search using maximum likelihood estimators (MLE); e.g. alternating projection (AP) [24] and expectation maximization (EM) [25].

Table I presents some general aspects that distinguish the AoA estimation algorithms from each other. The BF and SD algorithms can produce, directly, an angular spectrum by the means of matrix inversion and the eigen decomposition operation, respectively. The SRS and MLE algorithms, on the other hand, require an iterative optimization process. Furthermore, the BF and SD algorithms require many samples of the received signals to construct the system covariance matrix, the SRS and MLE algorithms, on the other hand, can provide the AoA estimates by utilizing few samples of the received signals. The main distinctive aspect, among all the algorithms, is the ability to estimate the AoA of correlated signals. This aspect is extremely important to resolve the multipath components. The algorithms that depend on the SRS and MLE optimization processes can estimate directly the AoA of correlated signals. The algorithms that depend on constructing the system's covariance matrix (i.e. the BF and SD algorithms) can estimate the AoA of correlated signals only by applying the spatial smoothing (SS) technique [26]. The SS technique decorrelates the received signals spatially, which causes a decrease in the array antenna degrees of freedom; i.e. the number of AoA estimations is less than the number of the array antenna elements. The SS technique may also demand a specific distribution of the array antenna elements in space. Finally, only the algorithms that depend on the MLE optimization process can jointly estimate the AoA and the received signal's amplitude for every individual signal's path. This feature can provide an indication of the most dominant path among several estimated paths.

Accordingly, we utilized here an algorithm that employs the MLE optimization process to estimate jointly the AoA and the signals' amplitudes of the direct and the reflected paths in a challenging urban environment. The algorithm does not require the SS technique to decorrelate received correlated

signals, thus, it does not reduce the array antenna degrees of freedom.

C. Contributions and Layout

In this paper, we introduce a comprehensive AoA estimation system for the LoRa communication network. Termed LoRa array (LoRay), the proposed system constitutes hardware and software solutions to estimate the AoA of the received signals in a real life urban environment. For the hardware part, we adopted the RTL-Array prototype [13] after extending it from 6 to 8 RF-channels. This extension increases the array angular response, hence, it increases the AoA estimation accuracy. For the software part, we adopted the space alternating generalized expectation-maximization (SAGE) algorithm [27] after modifying it to be suitable for the LoRa physical layer. The SAGE algorithm deploys the MLE optimization process to estimate the received signals' parameters. The SAGE algorithm can estimate the AoA of correlated signals efficiently based on few received signals' samples, therefore, it is suitable for estimating the AoA of the direct and the reflected paths of the received signal. Furthermore, the computational complexity of the SAGE algorithm (for a 1D AoA estimation problem) is very low, consequently, it can estimate the AoA of all the received signals in real-time.

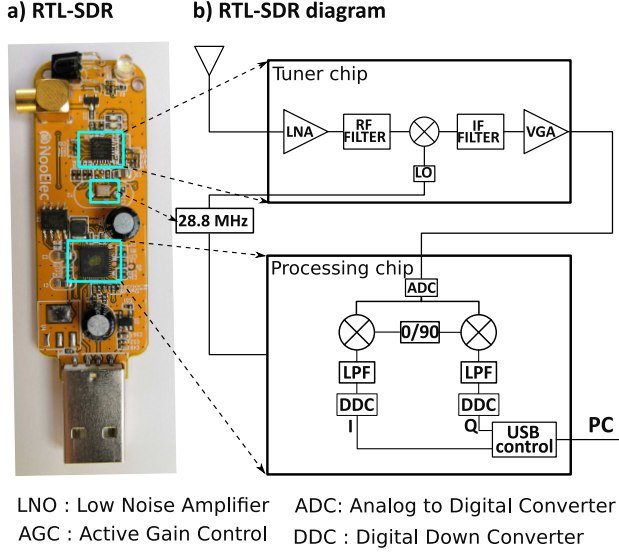
The contribution of this paper can be summarized as follows:

- i. We propose a comprehensive AoA estimation system that constitutes hardware and software implementations. The proposed system can estimate the AoA of the received signals in large scale urban environments. Moreover, the proposed system is suitable for LPWAN technologies in general and LoRa networks in specific.
- ii. The proposed hardware is cost effective (it is based on low cost hardware components); as opposed to the high cost hardware that has been deployed in [7], [9].
- iii. The proposed software is flexible (it does not impose any restrictions or assumptions). On the other hand, the solutions that were presented in [11], [12] assume that the signal is received from a LoS location with minimal multipath effect.
- iv. We provide a novel mathematical formulation of the LoRa physical layer with an array antenna frontend at the receiver side. We, furthermore, introduce a new modified SAGE algorithm that can utilize the orthogonality property of LoRa physical layer to retrieve the AoA of the received signals.
- v. Finally, we utilized the proposed system to conduct an extensive experimental analyses of the AoA estimation accuracy in complex urban environments. Both LoS and non-line-of-sight (NLoS) locations were studied and analyzed.

The remainder of the paper is structured as follows: In Sections II and III, the proposed hardware and software solutions are presented, respectively. The experimental results and analyses are presented in Sections IV and V. Finally, in Section VI, the conclusions are drawn.

TABLE I: A brief comparison of the existing AoA estimation algorithms

Aspects	BF	SD	SRS	MLE
Operation	direct	direct	iterative	iterative
Required samples	many	many	single or few	few
Correlated signals	possible with SS	possible with SS	directly	directly
Signals' amplitudes	no	no	no	yes


Fig. 2: An off-the-shelf RTL-SDR dongle.

II. THE LoRAY HARDWARE SOLUTION

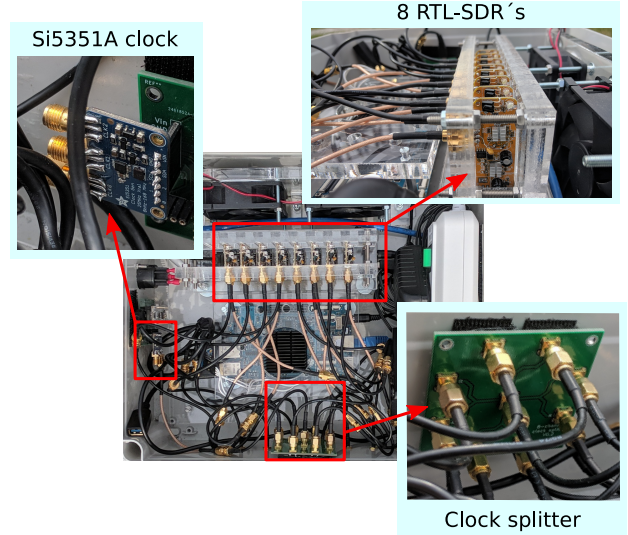
In this section, we present the complete hardware and software modifications that are required to convert multiple individual SDR frontends into a single SDR frontend with multiple RF-channels. The resultant RF-channels are synchronized in time and frequency, and coherent in phase. Furthermore, these RF-channels can be connected to any array antenna structure to provide beamforming and/or AoA estimation capabilities. The procedure is generic and it can be applied to any SDR frontend, in this paper however, we adopted the ultra low cost RTL-SDR dongle to provide a cost effective SDR frontend that constitutes multiple RF-channels.

In the following subsections, the time and frequency synchronization, and the phase calibration procedures will be presented, but first we will provide a brief introduction of the RTL-SDR dongle.

A. RTL-SDR

The RTL-SDR is a USB dongle that can be deployed as an RF-frontend as shown in Fig. 2(a). It operates at the frequency range of 24-1766 MHz [28], therefore, it is an ideal candidate for the LPWAN technologies that operate in the sub-1 GHz frequency band. The maximum sample rate of the RTL-SDR is 3.2 MS/s. However, samples will get lost at this rate. Mahalingam and Michelini [29] demonstrate that the maximum reliable sample rate is 2.85 MS/s.

The RTL-SDR has a simple design as shown in Fig. 2(b). The RF tuner chip contains a low noise amplifier (LNA)


Fig. 3: The LoRay frontend. The frontend consists primarily of 8 RTL-SDR dongles (the top right corner), an external clock generator (the top left corner) and a clock splitter (the bottom right corner). Furthermore, the LoRay frontend contains several active and passive cooling units.

followed by an RF image rejection filter. The tuner chip contains also a mixer that downconverts the RF signal into an intermediate frequency (IF). An IF filter and a variable gain amplifier (VGA) are implemented afterwards. The tuner chip sends the IF signal to the processing chip. This chip converts the analog signal into a digital signal using an 8 bit analog-to-digital converter (ADC). As well, an I/Q demodulation and a decimation processes are performed to convert the digital signal into a complex baseband signal. Finally the I/Q data passes through a USB control block that handles the transfer of the data to the computer.

Since the RTL-SDR is an RF frontend, it requires a software radio platform to operate as an SDR. Few RTL-SDR software radios have been developed in MATLAB [30] and GNU Radio² [31]. Software radio developers implemented few GNU Radio blocks that extract the I/Q data from the RTL-SDR such as the RTL-SDR source block or Multi-RTL source block. Nevertheless, most of them are derived or based upon the Osmocom source block [32].

²The GNU radio companion (GRC) is a free and open-source software development toolkit that provides signal processing blocks to implement software radios.

B. Time and Frequency Synchronization

The synchronization procedure of several RTL-SDR dongles in time and frequency can be divided into few steps as follows:

1) *Single Clock*: In order to synchronize several RTL-SDR dongles in time and frequency, they need to be connected to a single clock. Each individual RTL-SDR is driven with a quartz crystal oscillator that resonates at a frequency of 28.8 MHz, as shown in Fig. 2. The output signal of this crystal oscillator is capable of driving only a second RTL-SDR. Therefore, it is important to use a powerful external clock if more than two RF-channels are required.

For our LoRay frontend, we removed the crystal oscillator from every RTL-SDR then we distributed the clock signal from the external clock generator as shown in Fig. 3 (the left top corner). We chose the I²C programmable Si5351A clock generator [33] as the external clock to drive the 8 RTL-SDR dongles. The Si5351A clock generator has three independent non-coherent clock outputs. It can generate output signals with frequencies in the range of 8 kHz - 160 MHz. Furthermore, the signal of the clock generator has been divided into 8 signals using a customized clock splitter (the right bottom corner of Fig. 3). These 8 clock signals have been fed to every RTL-SDR dongle via SMA connectors.

2) *Symbol Synchronization*: After connecting all the RTL-SDR dongles to the same clock generator, as shown in Fig. 3, they are now synchronized in time and frequency domains. Nevertheless, a symbol synchronization process is still required. This is due to the different initiation time of every individual RTL-SDR, which is set by the host operating system. This can be adjusted by cross-correlating the RTL-SDR RF-channels to impose a symbol synchronization during the initialization process, as follows:

- 1) The first RF-channel x_1 is considered as a reference channel.
- 2) The log-likelihood function (LLF), for estimating the symbol delay of the n -th channel (x_n), can be expressed as [9], [34]

$$\Lambda [x_n(k)|\xi] \approx \left| \sum_{k=0}^{T_o} x_n(k)x_1^*(k-\xi) \right|, \quad (1)$$

where $()^*$ is the complex conjugate operator, $n = 2, 3, \dots, 8$ is the number of the RF-channels, k is the sampled time index, ξ is the symbol delay and T_o is the received signal duration.

- 3) By setting a range of possible values for ξ in (1), the symbol delay of the n -th channel (ξ_n) can be found as follows

$$\xi_n = \arg \max_{\xi} \Lambda [x_n(k)|\xi]. \quad (2)$$

3) *Dither process*: As mentioned before, the RTL-SDR software radio blocks have been implemented in GNU Radio. By default, these software blocks enable the dither process. The dither process is a technique that is used for digital signal processing to improve the performance of the ADC. However, for the RTL-SDR case, it is applied to improve the tuning accuracy of the local oscillator (LO). The dither process operates at each RTL-SDR individually, causing a random

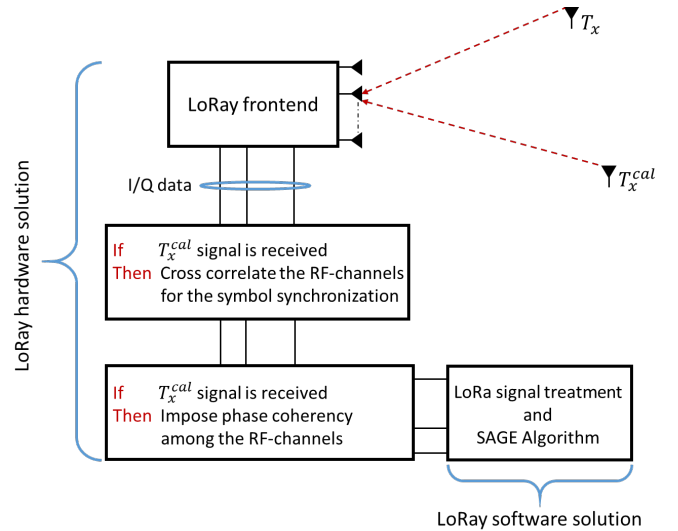


Fig. 4: A schematic representation of the LoRay system. Upon the LoRay frontend initialization, the calibration source T_x^{cal} transmits a calibration signal. The processing unit utilizes this calibration signal to start the symbol synchronization process. The cross-correlation process of the calibrating signals from all the receiving RF-channels is exploited for this purpose. Then, the phase calibration process will take place. It utilizes the direction information of the calibration source (should be known in advance) to impose the phase coherency state among the RF-channels. Afterwards, the LoRay system is ready to provide the AoA estimations of the received signals.

deviation of the IF signal. This leads to a continuous phase shift between the different RF-channels.

We used the Osmocom software block and the librtlsdr library [32]. This library enables the SDR function of the RTL chip. As mentioned above, the dithering process is enabled by default in this library. To ensure that the RTL-SDR dongles are operating at the exact time and frequency, the dither process should be disabled in the selected library.

C. Phase Calibration

Even though the local oscillators of all the RTL-SDR dongles are connected to the same clock, a phase calibration during the initialization process is required. This is due to the fact that the local oscillator of each RTL-SDR initializes with a random phase which varies from the other RTL-SDR dongles. In array antenna signal processing, there are several existing calibration methods to eliminate the initial random phase between the array antenna RF-channels [35].

One of the most used calibration techniques is the injection of a calibration signal into the signal path of each RTL-SDR. Upon the initialization of the device, the processing unit will use this injected signal to calibrate the phase. This calibration technique provides a high quality calibration signal for the circuitry behind the array antenna elements. Accordingly, this calibration technique does not calibrate for the antenna element patterns which might have significant variations due to mutual coupling, edge effects, and multipath propagation [35]. These variations of the elements' patterns will lead to an erroneous in the phase response of the array antenna.

Consequently, it will lead to a high AoA estimation error. The signal injection technique has been adopted by the coherent receiver project [36]. Due to the extra hardware modifications that are associated with this phase calibration technique³, the cost of this solution increases proportionally with the amount of the deployed RTL-SDR dongles.

In this paper, however, we adopted another calibration technique that utilizes a reference calibration source at a known location in the far field region. The calibration source transmits a calibration signal to all the array antenna elements. Upon the reception of this calibration signal, the processing unit will use this signal to calibrate the phase. Unlike the signal injection technique, this solution calibrates the phase of the array antenna against all abnormalities that might occur after the installation process. Furthermore, the deployment cost of this solution remain the same despite the amount of the deployed RTL-SDR dongles. For further information regarding the calibration process, the reader is referred to Monzingo et al. [35].

Fig. 4 shows a schematic representation of the calibration process of the LoRay system. The figure shows that the LoRay system, upon the reception of the calibration signal, will start the symbol synchronization and the phase calibration processes. Afterwards, the LoRay system is ready to provide the AoA estimates of the received signals.

III. THE LORAY SOFTWARE SOLUTION

The physical layer of the LoRa wide area network (LoRaWAN) is a closed source and proprietary, therefore, there are no official references or protocol specifications of the transmitted RF signal [37]. Accordingly, several research groups were busy in providing an understanding of the LoRa modulation scheme in the sub-1 GHz frequency band. Vangelista [38], for instance, has provided a mathematical model called frequency shift chirp modulation (FSCM) that can describe the LoRa modulation process. The same model has been adopted by Bernier et al. [39]. Knight and Seeber [37], Robyns et al. [40] and Ghanaatian et al. [41], on the other hand, have adopted a chirp spread spectrum (CSS) modulation based on the reverse engineering of the LoRaWAN's physical layer. Even though the LoRa modulation and demodulation processes have been intensively discussed in the literature [42]–[44], here, we will elaborate furthermore to provide a mathematical formulation for the LoRa physical layer when array antennas are used at the receiver side.

A. Signal Model

Assume a transmitted LoRa signal x_s reaches an array antenna system which is constructed of N antenna elements.

³For the case of [36]; they deployed (on top of the synchronization process in Section II-B) a noise source, an RF-splitter and RF-switches. They distributed the noise source signal to all the RF-channels using the RF-splitter, consequently, the noise source signal is utilized as a calibration signal. Finally, they deployed an RF-switch to every RF-channel. These switches are used to switch towards the noise source during the phase calibration process, afterwards, they switch back towards the array antenna.

Then, the received sampled signal vector at the time index k can be expressed as

$$\mathbf{x}(k) = [x_1(k) \dots x_n(k) \dots x_N(k)]^T, \quad (3)$$

in which

$$x_n(k) = rx_s(k - \tau)e^{i2\pi\Delta f k}e^{i\psi_n} + \omega_n(k), \quad (4)$$

where $()^T$ is the transpose notation, r is the received signal's amplitude, τ is the propagation time delay of the received sample $x_s(k)$, Δf is the frequency offset between the transmitter and the receiver, and $\omega_n(k)$ is the identically independently distributed (iid) complex-valued Gaussian noise with zero-mean and variance σ^2 ; i.e. $CN(0, \sigma^2)$. ψ_n is the phase difference between the n^{th} element in the array antenna and a reference point in the space. ψ_n is a function of θ and ϕ , where $\{\theta \in \mathbb{R} : -\pi \leq \theta \leq \pi\}$ is the azimuth angle and $\{\phi \in \mathbb{R} : 0 \leq \phi \leq \pi\}$ is the elevation angle. In this paper, however, we adopted the uniform linear array (ULA) antenna system, therefore, the phase response is expressed in terms of θ only, as follows

$$\psi_n(\theta) = \frac{2\pi}{\lambda}d_n \sin(\theta), \quad (5)$$

where λ is the operational wavelength and d_n is the displacement of the n -th antenna element with respect to a specific point in space. Different array antenna structure (such as a planar array or an array with randomly distributed antenna elements) can be deployed with the LoRay system. The comparison between various array antenna structures will constitute our future work.

The time and frequency synchronization⁴ of the received LoRa signal is out of this paper scope. Therefore, in the following, we will consider the simplified version of (4), as follows

$$x_n(k) = rx_s(k)e^{i\psi_n} + \omega_n(k), \quad (6)$$

The LoRa standard linear upchirp (also called a base chirp) can be expressed as [40]

$$x_s(k) = e^{i2\pi\left(\frac{\beta}{2K}k^2 + f_0k\right)}, \quad (7)$$

where $\beta \in \{125, 250 \text{ and } 500\}$ is the operational bandwidth of LoRa signal in the sub-1 GHz band, $K = 2^{\text{SF}}/\beta$ is the symbol duration and f_0 is initial frequency of the LoRa symbol that can be expressed as

$$f_0 = s \frac{\beta}{2^{\text{SF}}}, \quad (8)$$

$\text{SF} \in \{7, 8 \dots 12\}$ is the spreading factor and $s \in \{0, 1 \dots 2^{\text{SF}} - 1\}$ is the transmitted data symbol. Setting $s = 0$ will produce an upchirp signal, in which the frequency continuously increases during the symbol duration. The LoRa modulation uses the upchirp signal as a preamble for time and frequency synchronization process.

⁴The time and frequency synchronization procedure estimates the received signal parameters (i.e. τ and Δf). This procedure is crucial for the demodulation process [39], [41], and it does not affect the AoA estimation accuracy. That is due to the fact that these parameters are independent of the array antenna; see (4), therefore, they don't affect the phase difference vector (i.e. ψ_n) of the array antenna.

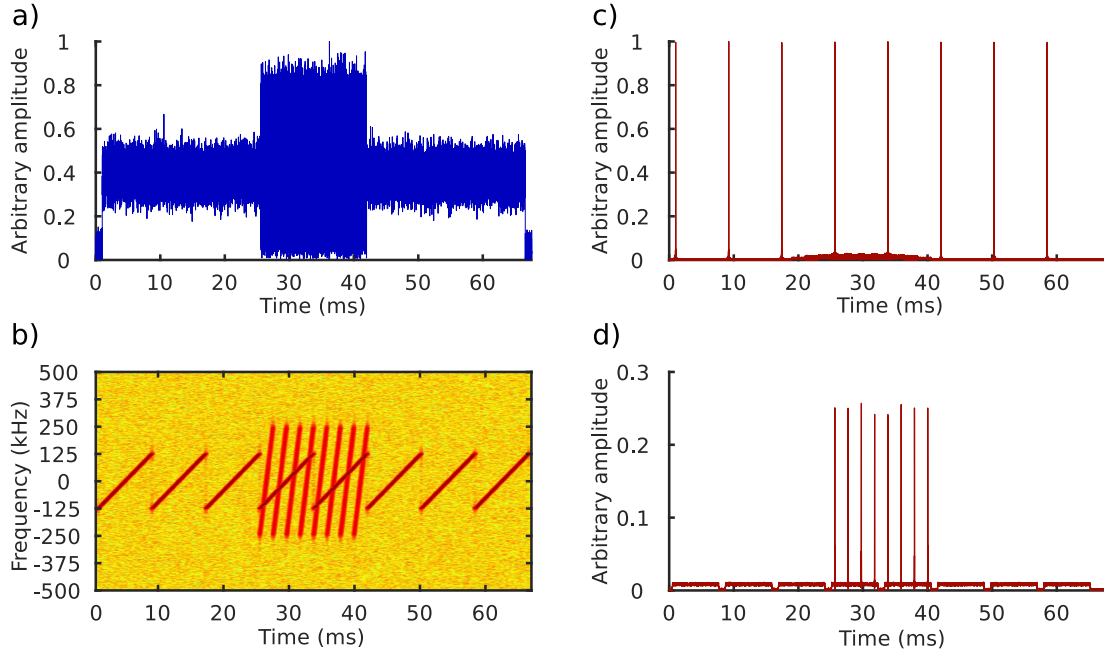


Fig. 5: Two simulated LoRa signals constitute 8 preamble (upchirp) symbols. The first signal (the long duration signal) has a bandwidth of 250 kHz and an SF of 11, while the second signal (the short duration signal) has a bandwidth of 500 kHz and an SF of 10. Figures a) and b) represent the combined simulated signals in time and in spectrogram (i.e. time and frequency) domains, respectively. It is clear that the two signals are interfering with each other. Figures c) and d) show the cross-correlation graphs, see (10), when the received signals have been cross-correlated with the base chirp of SF equals 11 and 10, respectively. One can deduce that the two signals can be distinguished correctly, even though they interfere with each other.

The model in (7) can also be presented as follows

$$x_s(k) = W_K^{\frac{\beta}{2}k^2 + Kf_0k}, \quad W_K = e^{i2\pi/K}, \quad (9)$$

which is the linearly cyclicly shifted versions of a base Zadoff-Chu (ZC) sequence [45]. The ZC sequence possesses a unique autocorrelation property, in which the periodic autocorrelation is orthogonal with all shifted replicas [46]. Therefore, LoRaWAN exploits this unique property to impose a random multiple access technique. Accordingly, an efficient utilization of the unlicensed spectrum can be obtained.

The cross-correlation between the received signals at the n -th antenna element and the base chirp leads to

$$\begin{aligned} z_n(\kappa) &= \frac{1}{K} \sum_{k=0}^{K-1} x_n(k) x_s^*(k + \kappa)_{\text{mod } K} \\ &= \frac{1}{K} \sum_{k=0}^{K-1} (r x_s(k) e^{i\psi_n} + \omega_n(k)) x_s^*(k + \kappa), \quad (10) \\ &= \begin{cases} r E_s e^{i\psi_n} + \nu_n(0) & \text{for } \kappa = 0 \\ \nu_n(\kappa) & \text{for } \kappa \neq 0 \end{cases} \end{aligned}$$

where E_s is the energy of the symbol x_s , and $\nu_n(\kappa)$ is the correlation between the complex noise and the base chirp, which can be expressed as

$$\begin{aligned} E_s &= \frac{1}{K} \sum_{k=0}^{K-1} x_s(k) x_s^*(k), \\ \nu_n(\kappa) &= \frac{1}{K} \sum_{k=0}^{K-1} \omega_n(k) x_s^*(k + \kappa), \end{aligned} \quad (11)$$

in which $\nu_n(\kappa) \sim CN(0, \sigma^2/K)$.

The cross-correlation function $z_n(\kappa)$, in (10), contains the appropriate phase response due to the antenna element displacement in space (i.e. ψ_n). Therefore, the received signal vector, see (3), will be substituted by the cross-correlation vector for the AoA estimation purposes, as follows

$$\mathbf{z} = [z_1(0) \dots z_n(0) \dots z_N(0)]^T. \quad (12)$$

Fig. 5 presents the simulation results of two simulated LoRa signals that constitute 8 preamble (upchirp) symbols. The first signal (the long duration signal) has a bandwidth of 250 kHz and an SF of 11, while the second signal (the short duration signal) has a bandwidth of 500 kHz and an SF of 10. Figs. 5(a) and 5(b) represent the combined simulated signals in time and in spectrogram (i.e. time and frequency) domains, respectively. It is clear that the two signals are interfering with each other. Figs. 5(c) and 5(d) show the cross-correlation graphs, see (10), when the simulated signals have been cross-correlated with the base chirp of SF equals 11 and 10, respectively. It is clear that the two signals can be distinguished correctly, even though they are interfering with each other. The unique orthogonality property of the ZC sequence allows the LoRaWAN to provide a multiple access technique in the sub-1 GHz frequency band. Consequently, as it will become apparent in Section IV, the phase response of every received signal can be retrieved individually.

B. SAGE Algorithm

As stated before, the SAGE algorithm employs the MLE optimization process to jointly estimate the received signals'

parameters [47]. It can estimate the AoA of highly correlated signals based on few received signals' samples, which makes it suitable for estimating the AoA of the direct and the reflected paths of the received signal. This capability is extremely important in urban environments, due to the presence of the intensive multipath effect. Furthermore, the computational complexity of the SAGE algorithm (for a 1D AoA estimation problem) is very low, therefore it can estimate the AoA of all the received signals in real time. There are many implementations of the SAGE algorithm, here, we adopted the implementation that is presented by Chung and Bohme [48]. Assuming there are M LoRa signals were generated in the far-field region, then, the received cross-correlation vector can be expressed as follows

$$\mathbf{z} = E_s \mathbf{D} \mathbf{r} + \boldsymbol{\nu}, \quad (13)$$

where $\mathbf{D} \in \mathbb{C}^{N \times M}$ and $\mathbf{r} \in \mathbb{C}^{M \times 1}$ are the steering matrix and the amplitudes vector of received signals, respectively, and $\boldsymbol{\nu} \in \mathbb{C}^{N \times 1}$ is the noise correlation vector. They can be expressed as follows

$$\begin{aligned} \mathbf{r} &= [r_1 \dots r_m \dots r_M]^T, \\ \mathbf{D} &= [\mathbf{d}(\theta_1) \dots \mathbf{d}(\theta_m) \dots \mathbf{d}(\theta_M)], \\ \boldsymbol{\nu} &= [\nu_1(0) \dots \nu_n(0) \dots \nu_N(0)]^T, \end{aligned} \quad (14)$$

where $\mathbf{d}(\theta_m) \in \mathbb{C}^{N \times 1}$ is the steering vector of the m -th received signal. For an ULA antenna, it can be expressed as

$$\mathbf{d}(\theta_m) = \begin{bmatrix} e^{i \frac{2\pi}{\lambda} d_1 \sin(\theta_m)} \\ \vdots \\ e^{i \frac{2\pi}{\lambda} d_n \sin(\theta_m)} \\ \vdots \\ e^{i \frac{2\pi}{\lambda} d_N \sin(\theta_m)} \end{bmatrix}. \quad (15)$$

The problem in (13) can be formulated as an optimization problem, the complete unobservable information, i.e. $\mathbf{D} \mathbf{r}$, needs to be estimated from the incomplete observable data, i.e. \mathbf{z} . To solve this optimization problem, the SAGE algorithm deploys expectation and maximization steps as follows:

The expectation step

$$\begin{aligned} \mathbf{z}_m &= \mathbf{E}[\mathbf{z}_m | \mathbf{z}, \boldsymbol{\eta}^\mu] \\ &= \mathbf{d}(\theta_m^\mu) r_m^\mu + (\mathbf{z} - \mathbf{D}^\mu \mathbf{r}^\mu), \end{aligned} \quad (16)$$

where $\boldsymbol{\eta}^\mu$ is the estimated parameters matrix and it is given by

$$\begin{aligned} \boldsymbol{\eta}^\mu &= [\eta_1^\mu \dots \eta_m^\mu \dots \eta_M^\mu] \\ \eta_m^\mu &= [\theta_m^\mu \quad r_m^\mu]^T, \end{aligned} \quad (17)$$

in which η_m^μ is the estimated parameters vector of the m -th received signal at the μ -th iteration step, and θ_m^μ and r_m^μ are the estimated θ_m and r_m at the μ -th iteration step, respectively. The covariance matrix of the expected m -th signal's cross-correlation vector can be expressed as

$$\mathbf{R}_m = \mathbf{z}_m \mathbf{z}_m^H, \quad (18)$$

where $()^H$ is the conjugate transpose notation. It is worth mentioning that the term $(\mathbf{z} - \mathbf{D}^\mu \mathbf{r}^\mu)$ in (16) represents the

mismatch between the expected values and the observed incomplete data, i.e. the noise in the system. Furthermore, the symbol energy E_s is included in the received signals' amplitude vector \mathbf{r}^μ

The maximization step

$$\begin{aligned} \theta_m^\mu &= \arg \max_{\theta} \{\mathbf{d}(\theta)^H \mathbf{R}_m \mathbf{d}(\theta)\} \\ r_m^\mu &= \frac{1}{N} \mathbf{d}(\theta_m^\mu)^H \mathbf{z}_m \end{aligned}, \quad (19)$$

The E-step in (16) is coupled iteratively with the M-step in (19), as shown in algorithm 1. The algorithm reveals that the parametric search is repeated iteratively until the parametric change satisfies a predefined tolerance ϵ .

In this paper, we utilized the estimated signals' amplitude vector \mathbf{r} to provide a confidence weight of the AoA estimation, as follows

$$w_{conf} = \frac{\max\{\mathbf{r}\}}{\sum_{m=1}^M r_m}, \quad (20)$$

this weight can provide an indication regarding the contribution of the strongest path compared with the other received paths. The confidence weight w_{conf} is always below 1 and it is relatively high, as will become apparent in Section V, for the direct paths. Thus, it can be used as an indicator of the AoA estimation's reliability. This is a very important feature that distinguishes the MLE-based AoA estimation algorithms from the AoA estimation algorithms that are based on the BF, SD and SRS techniques. The latter algorithms can not directly differentiate between the AoA of the direct and the reflected paths. Nevertheless, and especially for the NLoS conditions, it is important to install multiple spatially distributed AoA estimation systems (such as the LoRay system) to provide diverse AoA estimates which leads to a high estimation certainty.

Algorithm 1: SAGE Algorithm

Input: $\boldsymbol{\eta}^0$

- 1: $\mu \leftarrow 1$
- 2: **while** $\boldsymbol{\eta}^\mu - \boldsymbol{\eta}^{\mu-1} > \epsilon$ **do**
- 3: **for** $m \leftarrow 1$ to M **do**
- 4: **E-step :**
- 5: calculate \mathbf{z}_m , see (16)
- 6: calculate \mathbf{R}_m , see (18)
- 7: **M-step :**
- 8: estimate θ_m^μ and r_m^μ , see (19)
- 9: $\eta_m^\mu = [\theta_m^\mu \quad r_m^\mu]^T$
- 10: **end for**
- 11: $\mu \leftarrow \mu + 1$
- 12: **end while**

IV. LORAY PHASE RESPONSE

In section III, we presented the mathematical formulation of the LoRa modulation technique. We furthermore presented some simulation results to demonstrate the multiple access capability of the LoRa modulation. In this section, we will

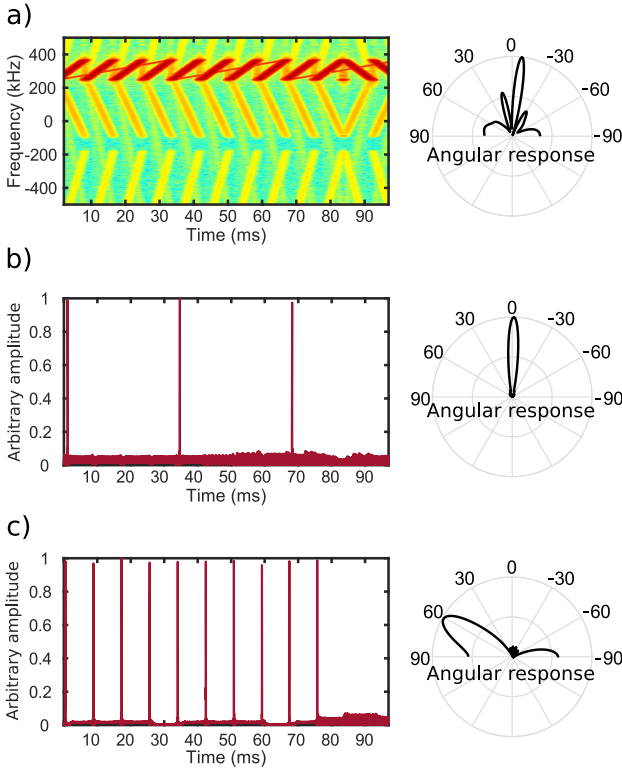


Fig. 6: The angular response of the LoRay system when two LoRa signals have been received simultaneously. The signals operate with a bandwidth of 125 kHz and an SF of 12 and 10, respectively. The two transmitters were placed at angles equal to 0° and 60° with reference to the LoRay system, respectively. Figure a) shows the spectrogram domain (the left figure) and the angular response (the right figure) for the two received signals directly; i.e. without the cross-correlation process in (10). Figures b) and c) show the received signals in the time domain (the left figures) and the associated angular responses (the right figures) after the cross-correlation process with an upchirp signal of SF equals 12 and 10, respectively.

demonstrate the proposed LoRay system’s capability of separating the phase response of two received LoRa signals simultaneously, and maintaining an accurate angular response for both signals.

We utilize, here, the response of the conventional beamformer (CBF) [16] (also known as Bartlett beamformer or delay and sum beamformer) to visualize the angular response of the received signal. The CBF response can be expressed as

$$\mathbb{A}(\theta) = \mathbf{d}(\theta)\mathbf{R}_a\mathbf{d}(\theta)^H, \quad (21)$$

where $\mathbf{R}_a \in \mathbb{C}^{N \times N}$ is the array covariance matrix.

We conducted an experiment in an anechoic chamber to test the LoRay system angular response in an ideal environment. The LoRay system was connected to an ULA antenna constructed of 8 elements with inter-element spacing is equal to half wavelength of the operating frequency. Two LoRa transceivers have been used to transmit two LoRa signals that have a bandwidth of 125 kHz and an SF of 12 and 10, respectively. The two transceivers have been placed within azimuthal angles equal to 0° and 60° with respect to the ULA. Fig. 6 shows the angular response of the LoRay system when two LoRa signals were received simultaneously. Fig.

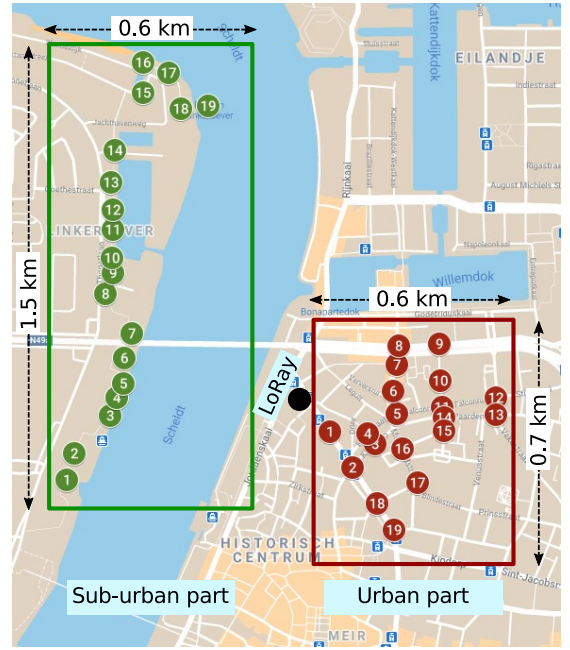


Fig. 7: Google Maps image of the measurement campaigns. The first measurement campaign has been conducted in the sub-urban part of the city, the green square. The second measurement campaign has been conducted in the urban part, the red square. The green and the red circles represent the transmitter locations in the sub-urban and urban parts, respectively. The black circle, on the other hand, represents the LoRay system location which is placed between the two measurement campaigns.

6(a) shows the spectrogram domain (the left figure) and the angular response (the right figure) for the two received signals directly; i.e. without the cross-correlation process in (10). The spectrogram figure shows a clear interference between the two signals. Accordingly, the angular response (the right figure) gives several peaks towards different directions. Figs. 6(b) and 6(c) show the received signals in the time domain (the left figures) and the associated angular responses (the right figures) after the cross-correlation process with an upchirp signal of SF equals 12 and 10, respectively. It is clear that the cross-correlation process, due to the orthogonal characteristic of the ZC sequence, can separate the two signals and their angular responses. Consequently, their AoA can be estimated separately.

V. EXPERIMENTAL RESULTS IN URBAN ENVIRONMENTS

We conducted two extensive measurement campaigns. For the both campaigns, the LoRay system was connected to an ULA antenna constructed of 8 elements with inter-element spacing of a half wavelength of the operating frequency. The ULA antenna was installed on the 8th floor of our research group building⁵, also known as the Beacon building in Antwerp city. The Beacon has a unique position, it is situated at the bank of the Scheldt river as shown in Fig.

⁵It is worth noting that multiple range and coverage experiments, for LoRaWAN technology [49], have been conducted when the gateways were installed at 5, 10 and 45 m above the ground. Therefore, the LoRay system installation, at approximately 24 m above the ground, can be considered within the realistic installation heights’ range of a typical LoRaWAN gateway.

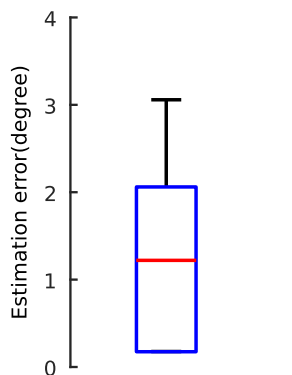


Fig. 8: The boxplot of the AoA estimation error of the 30 received signals from three different vegetation NLoS locations. The locations were in the sub-urban part of the city. Big trees were blocking the transmitter view from the LoRay system. The median and the maximum estimation error values were 1.26° and 3.05° , respectively.

7. The Scheldt river represents a natural barrier inside the city between the urban part (i.e narrow streets which are surrounded by tall buildings) and the sub-urban part (i.e. spacious areas where buildings are surrounded by large spaces and vegetation areas). This unique location of the Beacon allowed us to collect measurements with various scenarios, hence, we conducted a thorough study that investigates the accuracy of the AoA estimations inside cities.

The first measurement campaign has been conducted in the sub-urban part of the city, the green square in Fig. 7. This part constitutes mostly locations within either the LoS or the vegetation NLoS regions with respect to the LoRay system (60% of the total studied locations). The second measurement campaign has been conducted in the urban part, the red square in Fig. 7. This part constitutes mostly locations within the NLoS region with respect to the LoRay system (80% of the total studied locations). In both campaigns, 10 LoRa signals per location have been transmitted. A total 38 locations, divided equally between the two measurement campaigns, were studied. Therefore, the total amount of the received signals was 380 LoRa signals. The ground truth of the transmitter locations had been estimated using the global positioning system (GPS). The location estimation error of the GPS readings was within 10 m per location. In the following subsections, the presented AoA estimation error of the LoRay system is influenced by the ground truth error. This influence is inversely proportional to the distance between the transmitter and the LoRay system. For instance, the 10 meters error might lead up to 1.14° and 0.57° estimation error values when the transmitter is 500m and 1 km away from the LoRay system, respectively.

The transmitted LoRa signals have a bandwidth of 125 kHz and an SF of 12. The number of the unobservable received signals (i.e. M) was set to 5 signals. This number was chosen based on our empirical study of the urban environment, nevertheless, information theory techniques such as AIC and MDL [50] can be used to estimate the number of the receive signals M . The average computational time, for the SAGE algorithm to converge, was 10 ms using a PC with 2.60 GHz

Core i7 processor and 16 GB of RAM. In the following subsections, we will present our AoA estimation analyses for the aforementioned environments.

A. Vegetation NLoS Locations

Three locations, in the sub-urban part, were within the vegetation NLoS region. Big trees were blocking the transmitter view from the LoRay system. Fig. 8 shows the boxplot of the AoA estimation error for the 30 received signals from these vegetation NLoS locations. The AoA estimation of the strongest received path was considered. The central horizontal red mark, the bottom and top edges of the boxplot indicate the median, the 25th and 75th percentiles, respectively. The whiskers (the horizontal black mark) extend to the most extreme data points not considered the outliers, and the outliers (they exist only in Fig. 10) are plotted individually as red dots. Fig. 8 reveals that the AoA estimation was very accurate for the signals that arrived from the vegetation NLoS locations. The median and the maximum estimation error values were 1.26° and 3.05° , respectively. Furthermore, the estimation error for the vegetation NLoS locations was comparable to the estimation error for the LoS locations, as shown in Fig. 10. It is worth noting that the vegetation on hand was a typical vegetation that exist in the sub-urban part of a city. Therefore, the estimation error may increase if a forest-like vegetation is considered.

B. LoS versus NLoS Locations

In this subsection, we investigate the AoA estimation accuracy of the LoRay system for both LoS and NLoS conditions.

Fig. 9(a) shows the spectrogram, the cross-correlation graphs; see (10), and the angular response (the red plot) of a received signal from a location within the LoS region in the sub-urban part, respectively. The horizontal distance between this location and the LoRay system was around 1 km. The spectrogram and the cross-correlation graphs reveal that the LoRa signal can be received correctly from transmitters within the LoS region and are within one kilometer away from the receiver. Furthermore, the angular response of the received signal from a location within the LoS region has a single major lobe and it provides a maximum value towards the transmitter direction.

Fig. 9(b), on the other hand, shows the spectrogram, the cross-correlation graphs, and the angular response of a received signal from a location within the NLoS region in the urban part, respectively. The horizontal distance between this location and the LoRay system was around 310m, and around 10 buildings were blocking the transmitter view from the LoRay system. The spectrogram graph shows that the signal is completely below the noise floor and it can not be distinguished from the channel noise. Nevertheless, the cross-correlation graph shows that the orthogonality property of the ZC sequence can help in retrieving signals that are below the noise floor level. Furthermore, the angular response provides a maximum value towards the general direction of

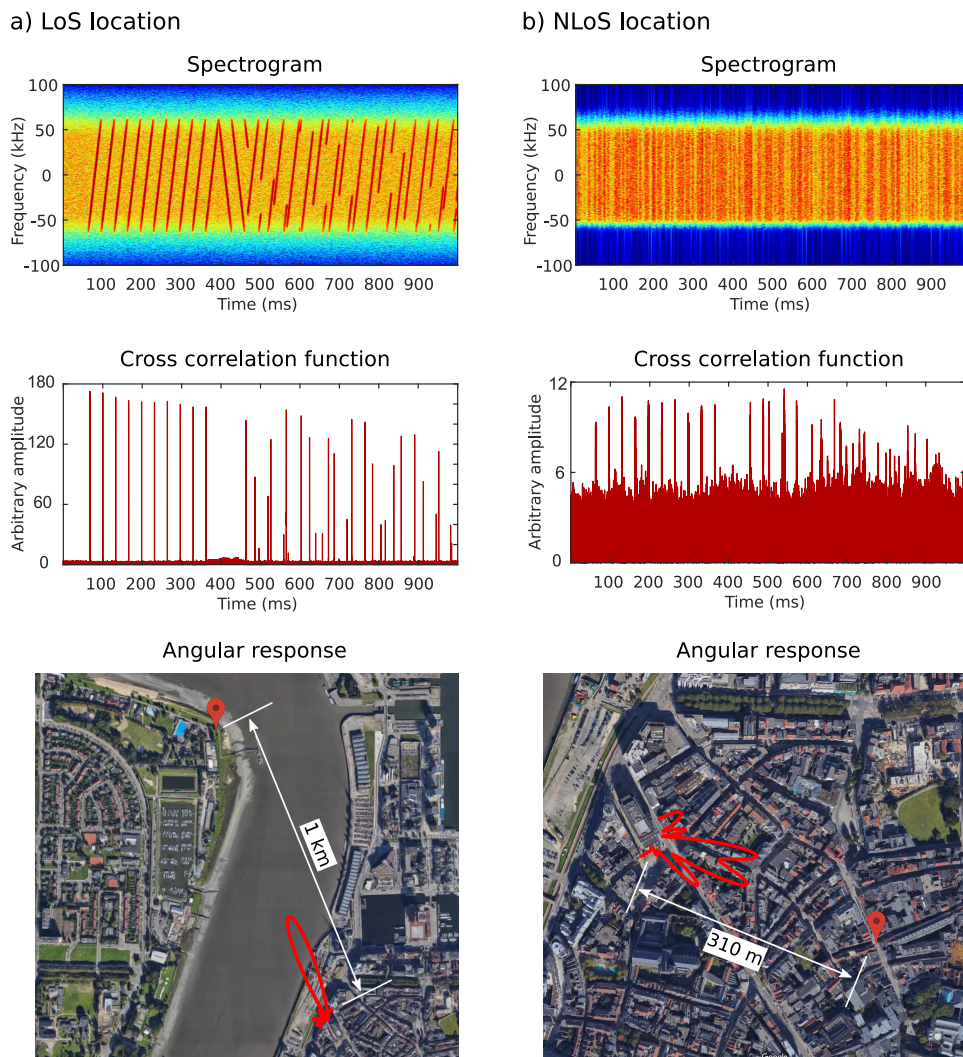


Fig. 9: Figures a) and b) show the spectrogram, the cross-correlation graphs; see (10), and the angular response of a received signal from a location within the LoS region in the sub-urban part and a location within the NLoS region in the urban part, respectively. The spectrogram and the cross-correlation graphs in figure a) reveals that the LoRa signal can be received correctly from transmitters within the LoS region and are within one kilometer away from the receiver. Furthermore, the angular response has a single major lobe and provides a maximum value towards the transmitter direction. For the NLoS location, the spectrogram graph in figure b) shows that the signal is completely below the noise floor and it can not be distinguished from the channel noise. Nevertheless, the cross-correlation graph in figure b) shows that the orthogonality property of the ZC sequence can help in retrieving signals that are below the noise floor level. Moreover, the angular response provides a maximum value towards the general direction of the transmitter location. Though, the maxima of the angular response is not unique.

the transmitter location. The maxima of the angular response is not unique, thus, the exact AoA can only be estimated using an AoA estimation algorithm, as presented in Section I-B.

Figs. 10(a) and 10(b) show the cumulative distribution function (CDF) and the boxplot (inner figures) for the AoA estimation error of all the received signals from the LoS and the NLoS locations, respectively. The AoA estimation of the strongest received path was considered. The AoA estimates of the received signals from the LoS locations was very accurate for both the sub-urban and urban environments. The maximum estimation error was around 3° for the both environments. This minor estimation error can be attributed to the erroneous in GPS readings, the human error factor during the LoRay system installation and the LoRay system estimation accuracy

in a realistic environment with the presence of the multipath effect. The AoA estimation of the received signals from the NLoS locations, on the other hand, had a higher estimation error. 80% of the received signals have been estimated within an estimation error below 10° . Nevertheless, there are few outliers which extended the estimation error up to 60° .

C. The Confidence Weight Indication

In this subsection, we utilized the confidence weight w_{conf} , see (20), to eliminate the unreliable AoA estimations. Figs. 11(a) and 11(b) show the confidence weight values versus the estimation error values for all the received signals from the LoS and the NLoS locations, respectively. The figure reveals that the direct paths from the LoS locations always dominate

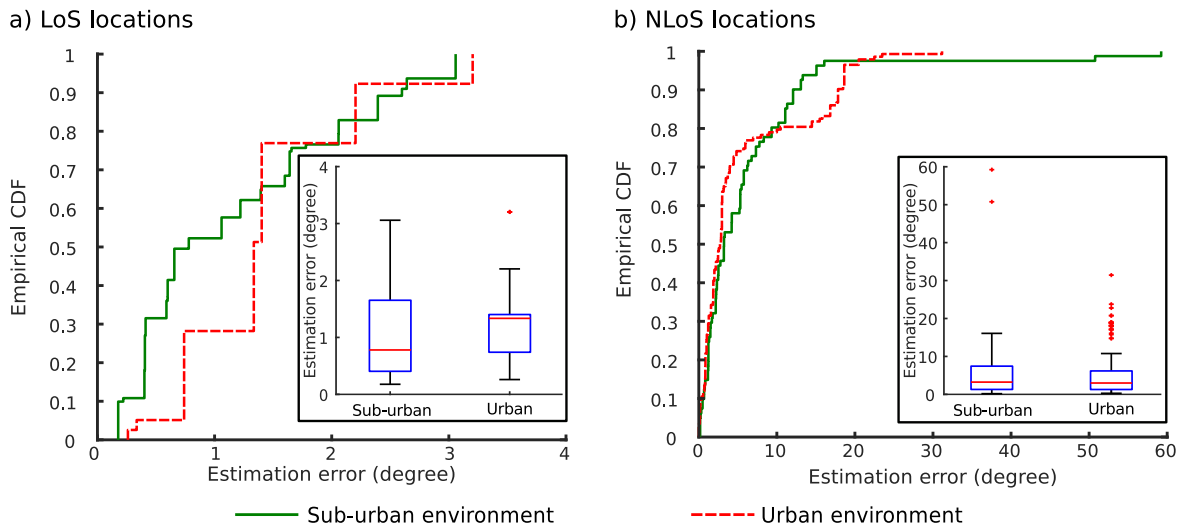


Fig. 10: The CDF and the boxplot (inner figures) for the AoA estimation error of all the received signals from the LoS and the NLoS locations, respectively. The maximum AoA estimation error from the LoS locations was around 3° for both the sub-urban and urban environments. 80% of the received signals from the NLoS locations were estimated with an estimation error below 10° .

the received signal's amplitude. Furthermore, all the paths with a high confidence weight from the NLoS locations exhibit low estimation error. On the other hand, paths with low confidence weights might exhibit high estimation error. Consequently, the confidence weight in (20) can provide an indication of the estimation reliability.

Fig. 12 shows the CDF plot of the AoA estimation error for all the received signals that have confidence weights greater than 0.5 for both environments. 85% of the total amount of the received signals have been used in this figure, of which 80% of them were estimated with an estimation error below 5° . It can be deduced that the deployment of the confidence weight threshold has eliminated signals with high AoA estimation error.

It is important to stress that the threshold value might eliminate an accurate AoA estimation. Furthermore, the threshold value for a certain environment should be calculated empirically. Therefore, and especially due to the NLoS conditions, it is important to install multiple spatially distributed AoA estimation systems (such as the LoRay system) in the vicinity of the transmitting devices to provide diverse AoA estimates, hence, achieving a high estimation certainty. Furthermore, combining the AoA estimates, that are supplied by these AoA estimation systems (see Fig. 1), can provide a location estimate of the transmitting device.

VI. CONCLUSION

In this paper, we introduced the LoRay system as a comprehensive AoA estimation solution that is suitable for LPWAN technologies in general and LoRa communication network in specific. The proposed system constitutes hardware and software solutions to estimate the AoA of the received signals in real life urban environments. The hardware solution is generic and it is applicable to any SDR that has a single RF-channel frontend, in this paper however, we utilized the ultra low cost RTL-SDR dongles. The software solution, on the other hand, utilizes the SAGE algorithm to jointly estimate

the AoA and the signals' amplitudes of the direct and the reflected paths. Furthermore, the signals' amplitudes have been exploited to provide an indication of the AoA estimation reliability.

We exploited the proposed system to conduct an extensive experimental analyses of the AoA estimation accuracy in a complex urban environment. The experimental results reveals that the proposed system provides very stable and accurate AoA estimates for both the LoS and the NLoS conditions. 80% of the received signals have been estimated within an estimation error below 2° and 10° for the LoS and the NLoS locations, respectively.

The proposed system is cost effective (it is constructed based on low cost hardware components), flexible (it does not impose any restrictions or assumptions), generic (it can be deployed with any array antenna structure), and computationally efficient (it can produce accurate AoA estimates of the received signals in the order of tens of milliseconds). Therefore, the LoRay system is a serious attempt that might lead to mass deployments of the AoA-based localization solutions for LPWAN technologies.

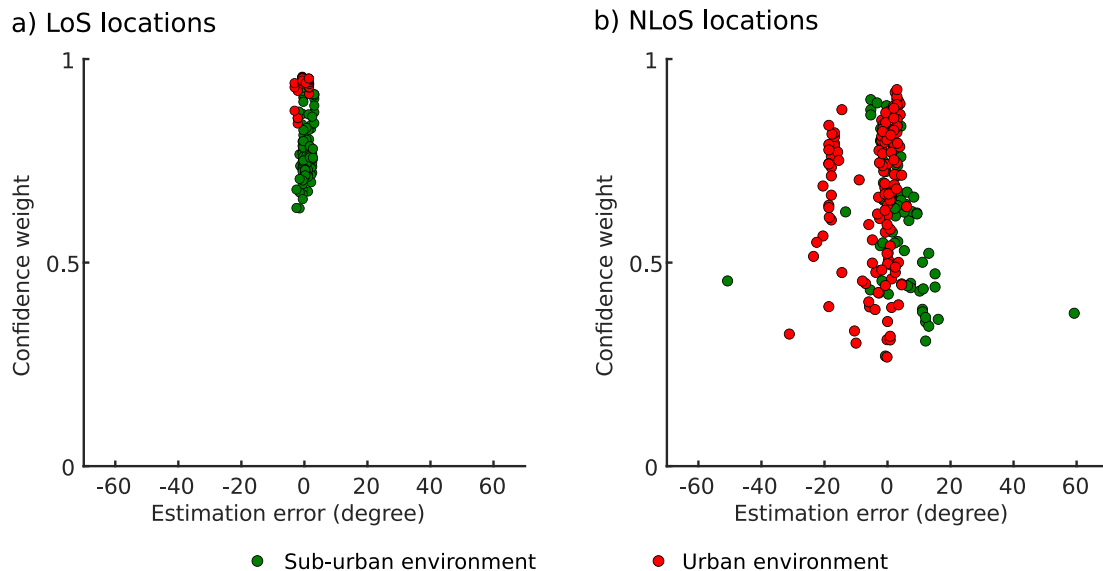


Fig. 11: The confidence weight; see (20), versus the estimation error for all the received signals from the LoS and NLoS locations, respectively. The figure reveals that the direct paths from all the LoS locations always dominate the received signal's amplitude. Furthermore, all the paths with a high confidence weight from the NLoS locations exhibit low estimation error. On the other hand, paths with low confidence weights might exhibit high estimation error.

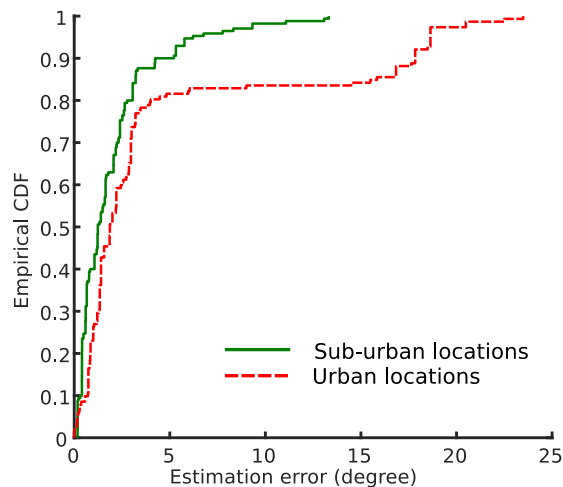


Fig. 12: The CDF plot of the estimation error for all the received signals that have confidence weights greater than 0.5 for the both environments. 85% of the total amount of the received signals have been used in this figure, of which 80% of them were estimated with an estimation error below 5° .

REFERENCES

- [1] M. Aernouts, B. Bellekens, R. Berkvens, and M. Weyn, "A comparison of signal strength localization methods with Sigfox," in *2018 15th Workshop on Positioning, Navigation and Communications (WPNC)*. IEEE, 2018, pp. 1–6.
- [2] T. Janssen, M. Weyn, and R. Berkvens, "A primer on real-world RSS-based outdoor NB-IoT localization," in *2020 International Conference on Localization and GNSS (ICL-GNSS)*. IEEE, 2020, pp. 1–6.
- [3] N. Podevijn, J. Trogh, A. Karaagac, J. Haxhibeqiri, J. Hoebeke, L. Martens, P. Suanet, K. Hendrikse, D. Plets, and W. Joseph, "TDoA-based outdoor positioning in a public LoRa network," in *12th European Conference on Antennas and Propagation (EuCAP 2018)*. IET, 2018, pp. 1–4.
- [4] M. Aernouts, N. BniLam, N. Podevijn, D. Plets, W. Joseph, R. Berkvens, and M. Weyn, "Combining TDoA and AoA with a particle filter in an outdoor network," in *2020 IEEE/ION Position, Location and Navigation Symposium (PLANS)*. IEEE, 2020, pp. 1060–1069.
- [5] M. Aernouts, N. BniLam, R. Berkvens, and M. Weyn, "TDoA: a combination of TDoA and AoA localization with LoRaWAN," *Internet of Things*, p. 100236, 2020.
- [6] N. BniLam, G. Ergeerts, D. Subotic, J. Steckel, and M. Weyn, "Adaptive probabilistic model using angle of arrival estimation for IoT indoor localization," in *2017 International Conference on Indoor Positioning and Indoor Navigation (IPIN)*. IEEE, 2017, pp. 1–7.
- [7] J. Steckel, D. Laurijssen, A. Schenck, N. BniLam, and M. Weyn, "Low-cost hardware platform for angle of arrival estimation using compressive sensing," in *12th European Conference on Antennas and Propagation (EuCAP 2018)*. IET, 2018, pp. 1–4.
- [8] "USRP B210," <https://www.ettus.com/all-products/ub210-kit/>, accessed: 2020-09-25.
- [9] N. BniLam, J. Steckel, and M. Weyn, "Synchronization of multiple independent subarray antennas: an application for angle of arrival estimation," *IEEE Transactions on Antennas and Propagation*, vol. 67, no. 2, pp. 1223–1232, 2019.
- [10] M. Weyn, G. Ergeerts, R. Berkvens, B. Wojciechowski, and Y. Tabakov, "DASH7 alliance protocol 1.0: Low-power, mid-range sensor and actuator communication," in *2015 IEEE Conference on Standards for Communications and Networking (CSCN)*. IEEE, 2015, pp. 54–59.
- [11] K.-J. Baik, S. Lee, and B.-J. Jang, "Hybrid RSSI-AoA positioning system with single time-modulated array receiver for LoRa IoT," in *2018 48th European Microwave Conference (EuMC)*. IEEE, 2018, pp. 1133–1136.
- [12] G. Avitabile, A. Florio, and G. Coviello, "Angle of arrival estimation through a full-hardware approach for adaptive beamforming," *IEEE Transactions on Circuits and Systems II: Express Briefs*, 2020.
- [13] N. BniLam, D. Joosens, J. Steckel, and M. Weyn, "Low cost aoa unit for IoT applications," in *2019 13th European Conference on Antennas and Propagation (EuCAP)*. IEEE, 2019, pp. 1–5.
- [14] "RTL-SDR," <https://www.rtl-sdr.com/>, accessed: 2020-09-30.
- [15] N. BniLam, E. Tanghe, J. Steckel, W. Joseph, and M. Weyn, "ANGLE: ANGular Location Estimation algorithms," *IEEE Access*, vol. 8, pp. 14 620–14 629, 2020.
- [16] H. L. Van Trees, *Optimum array processing: Part IV of detection, estimation, and modulation theory*. John Wiley & Sons, 2004.
- [17] R. Schmidt, "Multiple emitter location and signal parameter estimation," *IEEE Transactions on Antennas and Propagation*, vol. 34, no. 3, pp. 276–280, 1986.
- [18] A. Barabell, "Improving the resolution performance of eigenstructure-based direction-finding algorithms," in *ICASSP'83. IEEE International Conference on Acoustics, Speech, and Signal Processing*, vol. 8. IEEE, 1983, pp. 336–339.
- [19] R. Roy and T. Kailath, "ESPRIT-estimation of signal parameters via ro-

- tational invariance techniques,” *IEEE Transactions on Acoustics, Speech, and Signal Processing*, vol. 37, no. 7, pp. 984–995, 1989.
- [20] M. Haardt and J. A. Nosssek, “Unitary ESPRIT: How to obtain increased estimation accuracy with a reduced computational burden,” *IEEE Transactions on Signal Processing*, vol. 43, no. 5, pp. 1232–1242, 1995.
- [21] I. F. Gorodnitsky and B. D. Rao, “Sparse signal reconstruction from limited data using FOCUSS: A re-weighted minimum norm algorithm,” *IEEE Transactions on Signal Processing*, vol. 45, no. 3, pp. 600–616, 1997.
- [22] D. Malioutov, M. Cetin, and A. S. Willsky, “A sparse signal reconstruction perspective for source localization with sensor arrays,” *IEEE Transactions on Signal Processing*, vol. 53, no. 8, pp. 3010–3022, 2005.
- [23] A. Xenaki, P. Gerstoft, and K. Mosegaard, “Compressive beamforming,” *The Journal of the Acoustical Society of America*, vol. 136, no. 1, pp. 260–271, 2014.
- [24] I. Ziskind and M. Wax, “Maximum likelihood localization of multiple sources by alternating projection,” *IEEE Transactions on Acoustics, Speech, and Signal Processing*, vol. 36, no. 10, pp. 1553–1560, 1988.
- [25] M. I. Miller and D. R. Fuhrmann, “Maximum-likelihood narrow-band direction finding and the EM algorithm,” *IEEE Transactions on Acoustics, Speech, and Signal Processing*, vol. 38, no. 9, pp. 1560–1577, 1990.
- [26] T.-J. Shan, M. Wax, and T. Kailath, “On spatial smoothing for direction-of-arrival estimation of coherent signals,” *IEEE Transactions on Acoustics, Speech, and Signal Processing*, vol. 33, no. 4, pp. 806–811, 1985.
- [27] R. Thoma, D. Hampicke, A. Richter, G. Sommerkorn, A. Schneider, and U. Trautwein, “Channel parameter estimation in mobile radio environments using the SAGE algorithm,” *IEEE Transactions on Instrumentation and Measurement*, vol. 49, no. 2, pp. 357–364, 2000.
- [28] H. Mohamed, P. Lazaridis, D. Upton, U. Khan, B. Saeed, A. Jaber, Y. Zhang, P. Mather, M. F. Vieira, K. Barlee, *et al.*, “Partial discharge detection using low cost RTL-SDR model for wideband spectrum sensing,” in *2016 23rd International Conference on Telecommunications (ICT)*. IEEE, 2016, pp. 1–5.
- [29] D. Mahalingam and S. Michelini, “Analysis and evaluation of register transfer logic software defined radio performance,” *Degree of Bachelor of Science in Electrical and Computer Engineering, Massachusetts Institute of Technology*, 2016.
- [30] “MATLAB,” <https://nl.mathworks.com/products/matlab.html>, accessed: 2020-09-30.
- [31] “GNU Radio,” <https://www.gnuradio.org/>, accessed: 2020-09-30.
- [32] “Osmocom source block,” <https://osmocom.org/projects/gr-osmosdr/wiki>, accessed: 2020-09-30.
- [33] “Si5351A clock generator,” <https://cdn-learn.adafruit.com/downloads/pdf/adafruit-si5351-clock-generator-breakout.pdf?timestamp=1593318258>, accessed: 2020-09-30.
- [34] N. BniLam, J. Steckel, and M. Weyn, “Synchronization of multiple independent sub-array antennas for IoT applications,” in *12th European Conference on Antennas and Propagation (EuCAP 2018)*. IET, 2018, pp. 1–5.
- [35] R. A. Monzingo, R. L. Haupt, and T. W. Miller, “Introduction to adaptive arrays, scitech pub,” 2011.
- [36] “Coherent SDR,” <https://coherent-receiver.com/>, accessed: 2020-09-30.
- [37] M. Knight and B. Seeber, “Decoding LoRa: realizing a modern LPWAN with SDR,” in *Proceedings of the GNU Radio Conference*, vol. 1, no. 1, 2016.
- [38] L. Vangelista, “Frequency Shift Chirp Modulation: the LoRa modulation,” *IEEE Signal Processing Letters*, vol. 24, no. 12, pp. 1818–1821, 2017.
- [39] C. Bernier, F. Dehmas, and N. Deparis, “Low complexity LoRa frame synchronization for ultra-low power software-defined radios,” *IEEE Transactions on Communications*, vol. 68, no. 5, pp. 3140–3152, 2020.
- [40] P. Robyns, P. Quax, W. Lamotte, and W. Thenaers, “A multi-channel software decoder for the LoRa modulation scheme,” *IoTBDs 2018 - Proceedings of the 3rd International Conference on Internet of Things, Big Data and Security*, vol. 2018-March, no. July, pp. 41–51, 2018.
- [41] R. Ghanaatian, O. Afisiadis, M. Cotting, and A. Burg, “LoRa digital receiver analysis and implementation,” *ICASSP, IEEE International Conference on Acoustics, Speech and Signal Processing - Proceedings*, vol. 2019-May, pp. 1498–1502, 2019.
- [42] A. Marquet, N. Montavont, and G. Z. Papadopoulos, “Investigating theoretical performance and demodulation techniques for LoRa,” in *2019 IEEE 20th International Symposium on A World of Wireless, Mobile and Multimedia Networks (WoWMoM)*. IEEE, 2019, pp. 1–6.
- [43] J. Tapparel, O. Afisiadis, P. Mayoraz, A. Balatsoukas-Stimming, and A. Burg, “An open-source LoRa physical layer prototype on GNU radio,” *arXiv preprint arXiv:2002.08208*, 2020.
- [44] O. Afisiadis, M. Cotting, A. Burg, and A. Balatsoukas-Stimming, “On the error rate of the LoRa modulation with interference,” *IEEE Transactions on Wireless Communications*, vol. 19, no. 2, pp. 1292–1304, 2019.
- [45] B. Popovic, “Generalized chirp-like polyphase sequences with optimum correlation properties,” *IEEE Transactions on Information Theory*, vol. 38, no. 4, pp. 1406–1409, jul 1992. [Online]. Available: <http://ieeexplore.ieee.org/document/144727/>
- [46] M. Hua, M. Wang, K. W. Yang, and K. J. Zou, “Analysis of the frequency offset effect on Zadoff-Chu sequence timing performance,” *IEEE Transactions on Communications*, vol. 62, no. 11, pp. 4024–4039, 2014.
- [47] B. H. Fleury, M. Tschudin, R. Heddergott, D. Dahlhaus, and K. I. Pedersen, “Channel parameter estimation in mobile radio environments using the SAGE algorithm,” *IEEE Journal on Selected Areas in Communications*, vol. 17, no. 3, pp. 434–450, 1999.
- [48] P. J. Chung and J. F. Böhme, “DOA estimation using fast EM and SAGE algorithms,” *Signal Processing*, vol. 82, no. 11, pp. 1753–1762, 2002.
- [49] “LoRaWAN Range Part 2: Range and Coverage of LoRaWAN in Practice,” <https://smartmakers.io/en/lorawan-range-part-2-range-and-coverage-of-lorawan-in-practice/>, accessed: 2020-09-20.
- [50] M. Wax and T. Kailath, “Detection of signals by information theoretic criteria,” *IEEE Transactions on Acoustics, Speech, and Signal Processing*, vol. 33, no. 2, pp. 387–392, 1985.

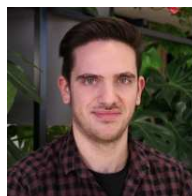


Noori BniLam received the M.Sc. degree in electronics and communication engineering from Baghdad University, Iraq, in 2012. In 2020 he received his first Ph.D. degree from Delft University of Technology, The Netherlands. His dissertation focused on devising analytical models and parameter estimation algorithms for renewable and green energy climate control systems.

Noori is currently a teacher assistant at the University of Antwerp, Belgium, where he is also pursuing his second Ph.D. degree at the IDLab - imec research group. His current research focuses on estimating the Angle of Arrival (AoA) of the received signals. Furthermore, his main objective is to develop AoA-based localization systems for Internet of Thing (IoT) applications. His research interests include (among others): adaptive array antenna signal processing, digital and analog beamforming, digital signal processing, modulation techniques, and optimization and parameter estimation algorithms.



Dennis Joosens received his Masters degree in Applied Engineering: Electronics-ICT from the University of Antwerp, in 2018. Currently, he is an overall hardware and software developer at the IDLab - imec research group.



Michiel Aernouts is a doctoral researcher at the University of Antwerp, Belgium. He received his Masters degree in Applied Engineering: Electronics-ICT from the University of Antwerp, in 2017. Currently, his Ph.D. research in the Internet Technology and Data Science Lab (IDLab - imec) research group is focused on context-aware localization in Low Power Wide Area Networks such as Sigfox, LoRaWAN and NB-IoT.



Jan Steckel received the M.Sc. degree in electronic engineering from the University College Karel de Grote—Hoboken, Antwerp Belgium, in 2007, and the Ph.D. degree from the Active Perception Laboratory, University of Antwerp, Antwerp, in 2012. His Ph.D. dissertation focused on array processing for in-air sonar systems drawing inspirations from biology. During this period, he developed the state-of-the-art sonar sensors, both biomimetic and sensorarray based. He was an Active Member of the Centre for Care Technology, University of Antwerp,

where he was in charge of various healthcare-related projects concerning novel sensor technologies. Furthermore, he pursued industrial exploitation of the patented 3-D array sonar sensor which was developed in collaboration with Prof. H. Peremans. In 2015, he joined the Constrained Systems Laboratory, University of Antwerp, as a Tenure-Track Professor, where he is involved in sensors, sensor arrays, and signal processing algorithms using an embedded, constrained systems approach. His current research interests include the industrial applications of ultrasonic sensing and development air-coupled ultrasonic imaging sensors. Results from the research of echolocating bats are transferred to radar systems. Finally, he works on pose estimation systems using sensor fusion techniques and various low-cost sensing modalities.



Maarten Weyn received his Ph.D. in Computer Science on the topic of Opportunistic Seamless Localization from the University of Antwerp, Belgium. He is a Professor at the University of Antwerp, teaching bachelor and master Mobile Communication, Telecommunication, Communication Systems, and Internet of Things: Low Power Embedded Communication in the department of Applied Sciences: Electronics-ICT. He is leading the low power communication and localization team at IDLab.